

Testing cosmic anisotropy with Pantheon sample and quasars at high redshifts

J. P. Hu¹, Y. Y. Wang¹, and F. Y. Wang^{1,2}

¹ School of Astronomy and Space Science, Nanjing University, Nanjing 210093, China
e-mail: fayinwang@nju.edu.cn

² Key Laboratory of Modern Astronomy and Astrophysics (Nanjing University), Ministry of Education, Nanjing 210093, China

Received date; accepted date

ABSTRACT

In this paper, we investigate the cosmic anisotropy from the SN-Q sample, consisting of the Pantheon sample and quasars, by employing the hemisphere comparison (HC) method and the dipole fitting (DF) method. Compared to the Pantheon sample, the new sample has a larger redshift range, a more homogeneous distribution, and a larger sample size. For the HC method, we find that the maximum anisotropy level is $AL_{max} = 0.142 \pm 0.026$ in the direction $(l, b) = (316.08^{+27.41}_{-129.48}, 4.53^{+26.29}_{-64.06})$. The magnitude of anisotropy is $A = (-8.46^{+4.34}_{-5.51}) \times 10^{-4}$ and the corresponding preferred direction points toward $(l, b) = (29.31^{+30.59}_{-30.54}, 71.40^{+9.79}_{-9.72})$ for the quasar sample from the DF method. The combined SN and quasar sample is consistent with the isotropy hypothesis. The distribution of the dataset might impact the preferred direction from the dipole results. The result is weakly dependent on the redshift from the redshift tomography analysis. There is no evidence of cosmic anisotropy in the SN-Q sample. Though some results obtained from the quasar sample are not consistent with the standard cosmological model, we still do not find any distinct evidence of cosmic anisotropy in the SN-Q sample.

Key words. supernovae: general – quasar – large-scale structure of Universe

1. Introduction

The Lambda cold dark matter model (Λ CDM) is consistent with most astronomical observations (Reid, et al. 2010; Trujillo-Gomez, et al. 2011; Bennett, et al. 2013; Hinshaw, et al. 2013; Planck Collaboration, et al. 2014b). The basis of the Λ CDM model assumes that the universe is homogeneous and isotropic on a large scale (Weinberg 1972, 2008). This hypothesis is known as the cosmological principle, and Clarkson & Maartens (2010) discuss the requirements in order to probe it. But several analyses of observations indicate that the universe may be anisotropic, for instance, these include quasar polarization vectors (Hutsemékers, et al. 2005), the fine-structure constant (Webb, et al. 2011; King, et al. 2012), the direct measure of the Hubble parameter (Bonvin, Durrer & Kunz 2006), the anisotropic dark energy (Koivisto & Mota 2008), the cosmic microwave background (CMB) (Tegmark, de Oliveira-Costa & Hamilton 2003; Bielewicz, Górski & Banday 2004; Eriksen, et al. 2004; Kim & Naselsky 2010b; Gruppuso, et al. 2011; Zhao 2014; Copi, et al. 2015; Akrami, et al. 2019), the large dipole of radio source counts (Singal 2011; Gibelyou & Huterer 2012; Rubart & Schwarz 2013; Tiwari & Nusser 2016; Colin, et al. 2017; Bengaly, Maartens & Santos 2018; Singal 2019), the quasar vector polarization alignment (Pelgrims & Hutsemékers 2016; Tiwari & Jain 2019), and the galaxy number counts in optical and IR wavelengths (Alonso, et al. 2015; Javanmardi & Kroupa 2017; Bengaly, et al. 2018). These works hint that the universe may have a preferred expanding direction (Perivolaropoulos 2014).

In recent years, type Ia supernovae (SNe Ia) (Amanullah, et al. 2010; Suzuki, et al. 2012; Betoule, et al. 2014; Scolnic, et al. 2018) have been widely employed to test cosmic isotropy. Antoniou & Perivolaropoulos (2010) searched for the preferred direc-

tion of anisotropy for the Union2 sample by adopting the hemisphere comparison (HC) method (Schwarz & Weinhorst 2007). They found a maximum accelerating expansion rate, which corresponds to a preferred direction of anisotropy. After that, Mariano and Perivolaropoulos (Mariano & Perivolaropoulos 2012) found a possible preferred anisotropic direction at the 2σ level using the Union2 sample, but by employing the dipole fitting (DF) method. Since then, these two methods have been widely used to explore the cosmic anisotropy (Cai & Tuo 2012; Cai, et al. 2013; Zhao, Wu & Zhang 2013; Li et al. 2013; Heneka, Marra & Amendola 2014; Bengaly, Bernui & Alcaniz 2015; Andrade, et al. 2018; Sun & Wang 2019) by investigating observational data of, for instance, the Union2.1 sample (Yang, Wang & Chu 2014; Javanmardi, et al. 2015; Lin, Li & Chang 2016), the Joint Light-Curve Analysis (JLA) sample (Lin et al. 2016; Chang, et al. 2018; Wang & Wang 2018), the Pantheon sample (Sun & Wang 2018), gamma-ray bursts (GRBs; Wang & Wang 2014), galaxies (Zhou, Zhao & Chang 2017), as well as gravitational wave and fast radio bursts (Qiang, Deng & Wei 2019; Cai, et al. 2019). Using HC and DF methods, Zhao, Zhou & Chang (2019) studied the cosmic anisotropy via the Pantheon sample. They found that the SDSS sample plays a decisive role in the Pantheon sample. It may imply that the inhomogeneous distribution has a significant effect on the cosmic anisotropy (Chang, et al. 2018). This opinion was also presented by Sun & Wang (2019). Their conclusions show that the effect of redshift on the result is weak and there is a negligible anisotropy when making a redshift tomography. Deng & Wei (2018) tested the cosmic anisotropy with the Pantheon sample, but by using the following three methods: the HC method, the DF method, and Healpix¹ (Górski, et

¹ <http://healpix.sourceforge.net>

al. 2005). They also performed a cross check. There are two preferred directions from the HC method. In adopting the DF method and Healpix, they found no noticeable anisotropy. They also compared the HC method with the DF method by using the JLA sample (Deng & Wei 2018) and found that the results of these two methods have not always been approximately coincident with each other. In order to better test the cosmic isotropy, the best way would be to add new samples with a relatively homogeneous distribution.

Quasars can be regarded as quasi-standard candles (Lusso & Risaliti 2017; Salvestrini, et al. 2019) by using the nonlinear relation (Avni & Tananbaum 1986; Lusso & Risaliti 2016) between the UV and X-ray monochromatic luminosities. Thus, the nonlinear relation can be used for cosmological purposes (Khodyachikh 1989; Qin, et al. 1997; Risaliti & Lusso 2015; Bisogni, Risaliti & Lusso 2017; Melia 2019; Khadka & Ratra 2020; Velten & Gomes 2020; Wei & Melia 2020; Lusso 2020). The quasar sample that consists of 1598 sources was built by Risaliti & Lusso (2019). They employed this sample to verify cosmological constraints. (Lusso, et al. 2019) and found that a deviation from the standard cosmological model emerges, with a statistical significance of 4σ . Whether this deviation will appear in cosmic isotropy is unclear. In this paper, we test the cosmological anisotropy from the SN-Q sample, which consists of the Pantheon sample and the quasar sample, by adopting the HC and DF methods. A fiducial value of $H_0 = 70 \text{ km s}^{-1} \text{ Mpc}^{-1}$ is adopted in this paper. The structure of the paper is as follows. In Section 2, we present the quasar sample and discuss the advantages of the SN-Q sample over the single Pantheon sample. The best-fitting values of the quasar and SN-Q samples are obtained by using the Markov chain Monte Carlo (MCMC) method. In Section 3, the HC and DF methods are given. By using these two methods, we investigate the cosmic anisotropy by employing the SN-Q sample. Finally, a brief summary is presented in the last section.

2. The observational data and MCMC fitting

2.1. The SNe Ia sample and the quasar sample

In this paper, we adopt the MCMC method provided by *emcee*² to explore the whole parameter space and investigate the cosmic anisotropy by using the Pantheon and quasar samples. The Pantheon sample, which was compiled by Scolnic, et al. (2018), contains 1048 SNe Ia covering the redshift range of $0.01 < z < 2.30$. The quasar sample consists of 1598 quasar sources (Risaliti & Lusso 2019): 1403 sources from SDSS DR7 (Shen, et al. 2011) and DR12 (Pâris, et al. 2017), 102 from XMM-COSMOS (Lusso, et al. 2010; Brusa, et al. 2010), 19 from ChaMP (Kalfountzou, et al. 2014), and 74 from other quasars (Shen, et al. 2011; Kalfountzou, et al. 2014; Vagnetti, Antonucci & Trevese 2013). Compared with the Pantheon sample, the quasar sample has a wider range of redshifts from $0.04 < z < 5.10$ and a larger size. Since some quasars have no coordinate information, we selected 1421 quasars as the final quasar sample, which covers a redshift of $0.11 < z < 4.13$. Combining the Pantheon and quasar samples, we obtain a new sample named the SN-Q sample. In Figure 1, the redshift cumulative distributions of the Pantheon, quasar, and SN-Q samples are given. In assessing the curve behaviors in Figure 1, we find that supernovae and quasars occupy forty-two percent and fifty-eight percent in the total sample, respectively. Ninety-five percent of the SN-Q sam-

ple distributes within $z = 2.3$. The distributions and corresponding densities of these three samples in the galactic coordinates are illustrated in Figure 2.

The cosmic anisotropy obtained from the SNe sample might rely on the inhomogeneous distribution of SNe Ia. The distributions of SNe Ia from the Pantheon sample are shown in panel (a) of Figure 2. It is obvious that the belt part (the SDSS sample) plays a major role in the full Pantheon sample. To make it easier to comprehend this focus, we plotted the density distribution of the Pantheon sample, which is shown in panel (b) of Figure 2. Zhao, Zhou & Chang (2019) analyzed the effect of the inhomogeneous distribution of the Pantheon sample on the cosmic anisotropy and found that the SDSS sample plays the most important role in the Pantheon sample. From panels (c) and (d) of Figure 2, we find that the distribution of the quasar sample is more homogeneous and its maximum density value is smaller than that of the Pantheon sample. Compared with the Pantheon sample, adding the quasar sample reduces the unevenness of the overall sample and weakens the decisive role of the SDSS subsample as shown in panels (e) and (f) of Figure 2. By combining Figures 1 and 2, we find that the SN-Q sample is better than the Pantheon sample in terms of quantity, redshift range, and the uniform of distribution. However, the unevenness may not have been eliminated. It is obvious that the data number of the North Galactic Hemisphere is larger than the South Galactic Hemisphere in the quasar sample. Through statistics, the data number of the South and North Galactic Hemispheres in the Pantheon sample, quasar sample, and SN-Q sample are (644, 404), (438, 983), and (1082, 1387), respectively. The same case also appears in the SN-Q sample. In order to neutralize the inhomogeneous Pantheon sample, it might be necessary to obtain a larger and more homogeneous sample.

2.2. The MCMC method

For the standard cosmological model, the theoretical distance modulus can be written as

$$\mu_{th} = 5 \log_{10} \frac{d_L}{\text{Mpc}} + 25, \quad (1)$$

where d_L is the luminosity distance. In the flat Λ CDM model, d_L can be calculated from

$$d_L = \frac{c(1+z)}{H_0} \int_0^z \frac{dz'}{\sqrt{\Omega_m(1+z')^3 + (1-\Omega_m)}}, \quad (2)$$

where c is the speed of light, H_0 is the Hubble constant, and Ω_m is the matter density. For SNe Ia, the best fitting value of Ω_m is achieved by minimizing the value of χ^2

$$\chi_{SN}^2 = \sum_{i=1}^{1048} \frac{(\mu_{obs}(z_i) - \mu_{th}(\Omega_m, z_i))^2}{\sigma^2}, \quad (3)$$

where $\sigma_i(z_i)$ is the observational uncertainty of the distance modulus.

For quasars, the relation between UV and X-ray luminosities can be parameterized as (Avni & Tananbaum 1986)

$$\log_{10}(L_X) = \gamma \log_{10}(L_{UV}) + \beta, \quad (4)$$

where L_X is the rest-frame monochromatic luminosity at 2 keV and L_{UV} is the luminosity at 2,500 Å. We note that γ and β are two free parameters. Considering $L = 4\pi d_L^2 F$, equation (4) can be written as

$$\log_{10}(4\pi d_L^2 F_X) = \gamma \log_{10}(4\pi d_L^2 F_{UV}) + \beta. \quad (5)$$

² <https://emcee.readthedocs.io/en/stable/>

From equation (5), we derive the theoretical X-ray flux (Khadka & Ratra 2020),

$$\begin{aligned}\phi([F_{UV}]_i, d_L[z_i]) &= \log_{10}(F_X) \\ &= \gamma(\log F_{UV}) + (\gamma - 1) \log 4\pi \\ &\quad + 2(\gamma - 1) \log_{10} d_L + \beta.\end{aligned}\quad (6)$$

For the quasar sample, the form of χ_Q^2 related to the X-ray flux F_X of the quasar is given as

$$\begin{aligned}\chi_Q^2 &= \sum_{i=1}^{1421} \left(\frac{(\log_{10}(F_X)_i - \phi([F_{UV}]_i, d_L[z_i]))^2}{s_i^2} \right. \\ &\quad \left. + \ln(2\pi s_i^2) \right),\end{aligned}\quad (7)$$

where the variance s_i^2 consists of the global intrinsic δ and the measurement error σ_i in $(F_X)_i$, that is, $s_i^2 \equiv \delta^2 + \sigma_i^2$. The function ϕ corresponds to the theoretical X-ray flux (equation (4)). Compared to δ and σ_i^2 , the error of $(F_{UV})_i$ is negligible.

In substituting equation (6) for equation (7) and minimizing the value of χ_Q^2 , we obtain the best-fit parameters: $\Omega_m = 0.74^{+0.22}_{-0.17}$, $\delta = 0.23^{+0.0046}_{-0.0044}$, $\gamma = 0.62^{+0.12}_{-0.10}$, and $\beta = 7.53^{+0.29}_{-0.35}$. It is important to note that Ω_m is in 4σ tension with the Λ CDM model (Risaliti & Lusso 2019). By combining equations (1), (3), (6), and (7), the χ^2 statistic for the SN-Q sample is

$$\begin{aligned}\chi_{Total}^2 &= \chi_{SN}^2 + \chi_Q^2 \\ &= \sum_{i=1}^{1048} \frac{(\mu_{obs}(z_i) - \mu_{th}(\Omega_m, z_i))^2}{\sigma^2} \\ &\quad + \sum_{i=1}^{1421} \left(\frac{(\log_{10}(F_X)_i - \phi([F_{UV}]_i, d_L[z_i]))^2}{s_i^2} \right. \\ &\quad \left. + \ln(2\pi s_i^2) \right).\end{aligned}\quad (8)$$

By using equation (8), the best-fit parameters are $\Omega_m = 0.29^{+0.0075}_{-0.0096}$, $\delta = 0.23^{+0.0046}_{-0.0057}$, $\gamma = 0.64^{+0.0089}_{-0.0115}$, and $\beta = 6.98^{+0.26}_{-0.36}$ from the SN-Q sample, which is shown in Figure 3. The result is consistent with the Λ CDM model.

From the best-fit parameters for the quasar and SN-Q samples, we find that when only considering the quasar sample, the matter density $\Omega_m = 0.74^{+0.22}_{-0.17}$. This is a significant departure from the Ω_m given by the standard cosmological model. But $\Omega_m = 0.29^{+0.0075}_{-0.0096}$ from the SN-Q sample is consistent with the standard cosmological model. This may imply that the quasars could not be used for the cosmological probe independently at present (Velten & Gomes 2020). It can be combined with others probes, for instance, SNe Ia, CMB, GRBs (Wang, Dai & Liang 2015), and fast radio bursts (Yu & Wang 2017).

3. Testing the cosmic anisotropy with the HC and DF methods

3.1. The HC method and results

The HC method was first proposed by Schwarz & Weinhorst (2007); it is widely used to investigate the cosmic anisotropy. For example, the anisotropy of cosmic expansion, the temperature anisotropy of the CMB (Bennett, et al. 2013; Eriksen, et al. 2004; Planck Collaboration, et al. 2014a; Akrami, et al. 2014; Hansen, Banday & Górski 2004; Quartin & Notari 2015), and the acceleration scale of modified Newtonian dynamics (Zhou, Zhao & Chang 2017; Chang, et al. 2018; Chang & Zhou 2019). Firstly, we briefly introduce this approach. Its goal is to identify

the direction, which corresponds to the axis of maximal asymmetry from the dataset, by comparing the accelerating expansion rate. In the spatially flat Λ CDM model, it is convenient to employ Ω_m to replace the accelerating expansion rate considering the relationship between the deceleration parameter q_0 and Ω_m . The most important step is to produce random directions $\hat{V}(l, b)$, which are used to split the dataset into two parts (defined as "up" and "down"), where $l \in (0^\circ, 360^\circ)$ and $b \in (-90^\circ, 90^\circ)$ are the longitude and latitude in the galactic coordinate system, respectively. According to "up" and "down" subdatasets, the corresponding best-fit values of $\Omega_{m,u}$ and $\Omega_{m,d}$ are obtained adopting the MCMC method. The nuisance parameters (δ , γ and β) are marginalized along with Ω_m in the MCMC process. The anisotropy level (AL) made up of $\Omega_{m,u}$ and $\Omega_{m,d}$ can be used to describe the accelerating expansion rate.

In this section, we adopt the HC method and use the SN-Q sample to study the cosmic anisotropy. The AL is defined as

$$AL = \frac{\Delta\Omega_m}{\bar{\Omega}_m} = 2 \times \frac{\Omega_{m,u} - \Omega_{m,d}}{\Omega_{m,u} + \Omega_{m,d}},\quad (9)$$

where $\Omega_{m,u}$ and $\Omega_{m,d}$ are the best-fit Ω_m of the "up" subset and "down" subset, respectively. These two subsets are distinguished from the full SN-Q sample by a random direction $\hat{V}(l, b)$. The 1σ uncertainty σ_{AL} is

$$\sigma_{AL} = \frac{\sqrt{\sigma_{\Omega_{m,u}}^2 + \sigma_{\Omega_{m,d}}^2}}{\Omega_{m,u} + \Omega_{m,d}}.\quad (10)$$

During the calculation, we repeated 3000 random directions $\hat{V}(l, b)$ for the HC method and the results are $\Omega_{m,u}^{\max} = 0.407$ and $\Omega_{m,d}^{\max} = 0.422$, and the corresponding errors are $\sigma_{\Omega_{m,d}^{\max}}^2 = 0.0149$ and $\sigma_{\Omega_{m,d}^{\max}}^2 = 0.0156$. Then, we obtain the 1σ uncertainty $\sigma_{AL} = 0.026$. The anisotropic level with 1σ uncertainty is

$$AL_{\max} = 0.142 \pm 0.026,\quad (11)$$

and the corresponding direction is

$$(l, b) = (316.08^{+27.41}_{-129.48}, 4.53^{+26.29}_{-64.06}).\quad (12)$$

The distribution of $AL(l, b)$ is shown in Figure 4. This preferred direction is inconsistent with the previous results with the Pantheon sample from the HC method. For instance, by employing the HC method, Deng & Wei (2018) obtained two preferred directions $(138.8^\circ, -6.8^\circ)$ and $(102.36^\circ, -28.58^\circ)$ from the Pantheon sample. In using the same sample, Sun & Wang (2018) and Zhao, Zhou & Chang (2019) achieved the HC preferred direction $(l, b) = (37^\circ, 33^\circ)$ and $(l, b) = (123.05^\circ, 4.78^\circ)$, respectively. These four directions are plotted in Figure 5. From the result of the HC method, it shows that the quasar sample has an obvious impact on the HC results.

We also assessed statistical significance of the results found by means of this test with simulated datasets. The simulated SN-Q datasets have the same direction in the sky as real data, but a different distance modulus (SNe Ia) and X-ray flux (quasar). Then the corresponding distance modulus and X-ray flux were constructed by the Gaussian function with the mean determined by equation (8), where $\Omega_m = 0.29$, $\delta = 0.23$, $\gamma = 0.64$, $\beta = 6.98$ is the best-fitting value to the SN-Q sample and the standard deviation equal to the corresponding real datapoint 1σ error. Therefore, we constructed 200 simulated datasets and obtain the corresponding AL_{\max} by employing the HC method. The distribution of AL_{\max} in these datasets was fitted by a Gaussian function with

the mean value 0.104 and the standard deviation 0.032, as shown in Figure 6. From Figure 6, we can find that the statistical significance of the maximum anisotropy level of AL_{max} , which is about 1.23σ and 14 percent of AL_{max} obtained from the simulated datasets, is greater than that of the real data. Therefore, the value of AL_{max} is not large enough. In addition, it is necessary to examine whether the maximum AL from the SN-Q sample is consistent with statistical isotropy. In order to determine this, we evenly redistributed the original data-sets across the sky and repeated it 200 times. The result of the simulated isotropic datasets is shown in Figure 7. The mean value is 0.099 and the standard deviation is 0.024. We note that 7 percent of AL_{max} obtained from the simulated isotropic datasets is larger than that of the real data. The statistical significance of AL_{max} is about 1.65σ . The results of the random and isotropic datasets are smaller than 2σ , which still supports the absence of significant anisotropy.

In the end of this subsection, we compare the HC preferred direction of the SN-Q sample with those derived in various observational datasets. In Figure 5, we plotted the preferred directions (l, b) found from various observational datasets by the HC method in the galactic coordinate system. From Figure 5, we find that the HC preferred direction in this paper is the deviation from that of the Pantheon sample and the SPARC galaxies sample, but it is generally consistent with those in the Union2 sample (Antoniou & Perivolaropoulos 2010; Cai & Tuo 2012; Chang & Lin 2015), the Union2.1 sample (Sun & Wang 2019; Lin, Li & Chang 2016), the Constitution sample (Sun & Wang 2019; Kalus, et al. 2013), and the JLA sample (Deng & Wei 2018). Overall, the distribution of the HC preferred direction obtained from a different sample is diffuse. As discussed by Sun & Wang (2019) and Zhao, Zhou & Chang (2019), the cosmic anisotropy found in the supernova sample significantly relies on the inhomogeneous distribution of SNe Ia in the sky. The preferred directions in various observational datasets are also shown in Table 1. From Table 1, we find that the HC preferred direction in this paper is also in agreement with the results of the CMB dipole (Lineweaver, et al. 1996), velocity flows (Watkins, Feldman & Hudson 2009; Feldman, Watkins & Hudson 2010), quasar alignment (Hutsemékers, et al. 2005, 2011; Hutsemékers & Lamy 2001), the CMB quadrupole (Bielewicz, Górski & Banday 2004; Frommert & Enßlin 2010), the CMB octopole (Bielewicz, Górski & Banday 2004), $\Delta\alpha/\alpha$ (Webb, et al. 2011; King, et al. 2012), and infrared galaxies (Yoon, et al. 2014; Bengaly, et al. 2017).

3.2. The DF method and results

The DF method is also used to test the cosmic anisotropy. Considering the dipole magnitude A and monopole term B , the theoretical distance modulus should be rewritten as

$$\tilde{\mu}_{th} = \mu_{th} \times (1 + A(\hat{\mathbf{n}} \cdot \hat{\mathbf{p}}) + B), \quad (13)$$

where $\hat{\mathbf{n}}$ and $\hat{\mathbf{p}}$ correspond to the dipole direction and the unit vector pointing to the position of the SN Ia or quasar, respectively. In the galactic coordinate, $\hat{\mathbf{n}}$ is written as

$$\hat{\mathbf{n}} = \cos(b) \cos(l) \hat{\mathbf{i}} + \cos(b) \sin(l) \hat{\mathbf{j}} + \sin(b) \hat{\mathbf{k}}. \quad (14)$$

For any $i_{th}(l_i, b_i)$ data points, $\hat{\mathbf{p}}$ is given by

$$\hat{\mathbf{p}} = \cos(b_i) \cos(l_i) \hat{\mathbf{i}} + \cos(b_i) \sin(l_i) \hat{\mathbf{j}} + \sin(b_i) \hat{\mathbf{k}}. \quad (15)$$

We were able to obtain the best-fit dipole direction (l, b) by substituting equation (13) for equation (3) and minimizing χ^2 .

Equation (13) can be directly used for the SNe Ia sample. For the quasars, according to equation (1), the theoretical distance modulus can also be written as

$$\tilde{\mu}_{th} = 5 \log_{10} \frac{d_L}{\text{Mpc}} + 25. \quad (16)$$

In substituting equation 16 for equation 13, we obtain

$$\log_{10} \frac{d_L}{\text{Mpc}} = (\log_{10} \frac{d_L}{\text{Mpc}} + 5) \times (1 + A(\hat{\mathbf{n}} \cdot \hat{\mathbf{p}}) + B) - 5. \quad (17)$$

Thus the theoretical X-ray flux with dipole and monopole corrections is given by

$$\begin{aligned} \tilde{\phi}([F_{UV}]_i, d_L[z_i]) &= \gamma(\log F_{UV}) + (\gamma - 1) \log 4\pi + \beta \\ &+ 2(\gamma - 1) \left(\log_{10} \frac{d_L}{\text{Mpc}} + 5 \right) \\ &\times (1 + A(\hat{\mathbf{n}} \cdot \hat{\mathbf{p}}) + B) - 5. \end{aligned} \quad (18)$$

Adding equations (13) and (18) to (8) and minimizing the value of χ^2_{Total} , the marginalized posterior distribution for the SN-Q sample is shown in Figure 8. In total, there are eight parameters in the DF method, four of which are used to describe the universal anisotropy, that is, l , b , A , and B . The results show that the dipole direction (l, b) is $(327.21^{+28.24}_{-27.50}, 48.67^{+8.99}_{-8.54})$, the dipole magnitude $A = (-4.36^{+1.98}_{-2.74}) \times 10^{-4}$ and the monopole term $B = (-6.60^{+21.5}_{-28.6}) \times 10^{-5}$. The dipole direction is generally consistent with the preferred direction $(316.08^{+27.41}_{-129.48}, 4.53^{+26.29}_{-64.06})$ of the HC method. Both the dipole magnitude A and monopole term B are approximately equal to zero, indicating that there is no significant anisotropy in the SN-Q sample. Next, we carry out a redshift tomography analysis to discuss the effect of redshift. The results of the redshift tomography analysis were calculated, as shown in Table 2. Based on analyses of Figure 1, the number of low redshift sources is relatively large, so the redshift intervals are not uniform in the redshift tomography analysis. From the results of redshift tomography, it can be found that the dipole directions are distributed in a relatively small range. The maximum of monopole term A and the dipole magnitude B are near zero. There is no significant change in the dipole direction and anisotropic level with different redshift ranges. We note that $|A|$ and $|B|$ of the first bin are larger than that of others bins. This indicates that the anisotropy level of the low redshift range might be relatively higher.

At the end of this section, we make a comparison between the dipole directions of the SN-Q sample with that derived from other samples and compare the results between the HC method and the DF method for the same sample. At first, we marked the dipole directions obtained from different samples in the galactic coordinate system, as shown in Figure 5. The dipole directions obtained from different samples are mostly located in a relatively small part of the South Galactic Hemisphere. The dipole direction in this paper is inconsistent with them. The longitude l is close, but the deviation of latitude b is large. It might be caused by the inhomogeneous distribution of SNe Ia, as discussed in Section 2.1. The data number of the SN-Q sample in the North Galactic Hemisphere is larger than that in the South Galactic Hemisphere. But the dipole direction is in agreement with the results derived for the CMB dipole, velocity flows, quasar alignment, the CMB quadrupole, the CMB octopole, and $\Delta\alpha/\alpha$. For the same sample, we find that the results of these two methods are not always consistent with each other. For instance, these two preferred directions obtained by the HC and DF methods in the SPARC galaxies sample (Zhou, Zhao & Chang 2017; Chang,

et al. 2018), the Union2 sample (Antoniou & Perivolaropoulos 2010; Mariano & Perivolaropoulos 2012; Cai & Tuo 2012; Cai, et al. 2013; Chang & Lin 2015), and the JLA sample (Bengaly, Bernui & Alcaniz 2015; Sun & Wang 2019; Lin et al. 2016; Deng & Wei 2018), are consistent. However, the HC and DF preferred directions obtained from the Constitution sample (Sun & Wang 2019; Kalus, et al. 2013) are inconsistent. The same case is also exhibited in the Pantheon sample (Sun & Wang 2018; Zhao, Zhou & Chang 2019; Deng & Wei 2018). This may be due to the sensitivity of the two methods (Chang & Lin 2015).

In Table 1, we summarize the preferred directions (l , b) found in different cosmological models using different methods and observational datasets. The parts of the DF method and HC method have been discussed at the beginning of this section. In addition, we also summarize the research results obtained by various methods for different models (Λ CDM, w CDM, and CPL). Looking through the results from the same sample, we find that the results are almost independent of these three models.

4. Summary

The cosmic principle assumes that the universe is homogeneous and isotropic on cosmic scales. The research on cosmic anisotropy from SNe Ia also shows that there is no obvious anisotropy. In this work, we test the cosmic anisotropy with a new sample, which consists of SNe Ia and the quasars, by using the HC and DF methods. Nevertheless, the results show that there is no obvious anisotropy.

Firstly, we briefly investigate the Pantheon sample and quasar sample. By assessing the results, we find that adding the quasar sample reduces the unevenness of the overall sample. Compared with the Pantheon sample, the new sample (SN-Q sample) has a larger size, wider range of redshift, and a more uniform distribution. But the distribution of the SN-Q sample is still inhomogeneous in the North Galactic Hemisphere and South Galactic Hemisphere. We also briefly discuss the effect of inhomogeneous distribution on the dipole preferred in the SN-Q sample. By adopting the MCMC method, we obtain the best fitting values of Ω_m , δ , γ , β , and H_0 and find that 4σ tensions exist between the best-fit value of Ω_m from the quasar sample and that of the Λ CDM model. Then, by adding the Pantheon sample into the quasar sample, the 4σ tension disappears.

For the HC method, the preferred direction that corresponds to the maximum accelerating expansion is $316.08^{+27.41}_{-129.48}$, $4.53^{+26.51}_{-64.06}$. The anisotropy level AL_{\max} is equal to 0.142 ± 0.026 . By using the simulated datasets, we assess the HC result and determine that the statistical significance is about 1.23σ . In addition, we also examine whether the AL_{\max} from the SN-Q sample is consistent with statistical isotropy by employing the simulated isotropic datasets. The statistical significance is about 1.65σ . The results show that it is hardly reproduced by simulated datasets or isotropy simulated datasets. For the DF method, we find that the preferred direction in the SN-Q sample points toward $(327.21^{+28.24}_{-27.50}, 48.67^{+8.99}_{-8.54})$ with an anisotropy level of $A = (-4.36^{+1.98}_{-2.74}) \times 10^{-4}$, which is marginally consistent with the result of the HC method. There is a considerable deviation for the latitude direction l from those obtained from other SNe Ia samples, which may be caused by including the quasar sample. The preferred directions obtained by using the HC method and the DF method from the SN-Q sample are both in agreement with the results of the CMB dipole, velocity flows, quasar alignment, the CMB quadrupole, the CMB octopole, and $\Delta\alpha/\alpha$. The results of the redshift tomographic analysis show that the dipole

direction is weakly dependent on redshift. Comparing this with previous studies of the Pantheon sample, the preferred directions in the SN-Q sample have an obvious divergence. There does not exist an obvious anisotropy from the SN-Q sample.

Although the SN-Q sample is better than the Pantheon sample in some aspects, such as the quantity, redshift range, and uniform of distribution, there are still some shortcomings. For example, the distribution of the SN-Q sample is not uniform in the whole sky. Next-generation X-ray surveys, such as eROSITA, will provide us with larger and more precise luminosity distance determinations of quasars, so that we should be able to reduce the uncertainties obtained in our analysis. By employing a simulated e-ROSITA quasar sample, predictions for e-ROSITA from a quasar Hubble diagram have been made by Lusso (2020). Colin, et al. (2019) point out that the cosmic acceleration is due to a non-negligible dipole anisotropy by analyzing the JLA sample. We think that the same research can be performed by a combined sample of SNe Ia and quasars, considering the quasar sample enables us to talk about this study in a higher redshift range and to test whether the same result will still be obtained. This will be pursued in future work.

Acknowledgements. We thank the anonymous referee for valuable comments. This work is supported by the National Natural Science Foundation of China (grant U1831207).

References

- Akrami Y., et al. [Planck], [arXiv:1906.02552 [astro-ph.CO]]
 Akrami Y., et al. 2014, ApJL, 784, L42
 Alonso A. L., et al. 2015, MNRAS, 449, 670-684
 Amanullah R., et al. 2010, ApJ, 716, 712
 Andrade U., Bengaly C. A. P., Alcaniz J. S. & Santos B. 2018, PhRvD, 97, 083518
 Antoniou I. & Perivolaropoulos L. 2010, JCAP, 2010, 012
 Avni Y. & Tananbaum H. 1986, ApJ, 305, 83
 Bengaly C. A. P., Bernui A. & Alcaniz J. S. 2015, ApJ, 808, 39
 Bengaly C. A. P., et al. 2017, MNRAS, 464, 768
 Bengaly C. A. P., et al. 2018, MNRAS, 475, L106-L110
 Bengaly C. A. P., Maartens R. & Santos M. G., 2018, JCAP, 04, 031
 Bennett C. L., et al. 2013, ApJS, 208, 20
 Betoule M., et al. 2014, A&A, 568, A22
 Bielewicz P., Górski K. M. & Banday A. J. 2004, MNRAS, 355, 1283
 Bisogni S., Risaliti G. & Lusso E. 2017, FrASS, 4, 68
 Bonvin C., Durrer R. & Kunz M. 2006, PhRvL, 96, 191302
 Brusa M., et al. 2010, ApJ, 716, 348
 Cai R.-G., Liu T.-B., Wang S.-J. & Xu W.-T. 2019, JCAP, 2019, 016
 Cai R.-G., Ma Y.-Z., Tang B. & Tuo Z.-L. 2013, PhRvD, 87, 123522
 Cai R.-G. & Tuo Z.-L. 2012, JCAP, 2012, 004
 Chang Z. & Lin H.-N. 2015, MNRAS, 446, 2952
 Chang Z., Lin H.-N., Sang Y. & Wang S. 2018, MNRAS, 478, 3633
 Chang Z., Lin H.-N., Zhao Z.-C. & Zhou Y. 2018, ChPhC, 42, 115103
 Chang Z. & Zhou Y. 2019, MNRAS, 486, 1658
 Clarkon C. & Maartens R., 2010, CQG, 27, 124008
 Colin J., Mohayaee R., Rameez M. & Sarkar S., 2017, MNRAS, 471, 1045-1055
 Colin J., Mohayaee R., Rameez M. & Sarkar S., A&A, 2019 631, L13
 Colin J., Mohayaee R., Sarkar S. & Shafieloo A. 2011, MNRAS, 414, 264
 Copi C. J., Huterer D., Schwarz D. J. & Starkman G. D. 2015, MNRAS, 449, 3458
 Deng H.-K. & Wei H. 2018, EPJC, 78, 755
 Deng H.-K. & Wei H. 2018, PhRvD, 97, 123515
 Eriksen H. K., et al. 2004, ApJ, 605, 14
 Feindt U., et al., 2013, A&A, 560, A90
 Feldman H. A., Watkins R. & Hudson M. J. 2010, MNRAS, 407, 2328
 Frommert M. & Enßlin T. A. 2010, MNRAS, 403, 1739
 Gibelyou C. & Huterer D., 2012, MNRAS 427, 1994-2021
 Górski K. M., et al. 2005, ApJ, 622, 759
 Gruppiso A., et al. 2011, MNRAS, 411, 1445
 Hansen F. K., Banday A. J. & Górski K. M. 2004, MNRAS, 354, 641
 Heneka C., Marra V. & Amendola L. 2014, MNRAS, 439, 1855
 Hinshaw G., et al. 2013, ApJS, 208, 19
 Hutsemékers D., Cabanac R., Lamy H. & Sluse D. 2005, A&A, 441, 915
 Hutsemékers D. & Lamy H. 2001, A&A, 367, 381

- Hutsemékers D., et al. 2011, ASPC, 441, ASPC.449
- Javanmardi B. & Kroupa P., 2017, A&A, 597, A120
- Javanmardi B., Porciani C., Kroupa P. & Pflamm-Altenburg J. 2015, ApJ, 810, 47
- Kalfountzou E., et al. 2014, MNRAS, 445, 1430
- Kalus B., Schwarz D. J., Seikel M. & Wiegand A. 2013, A&A, 553, A56
- Kazantzidis L. & Perivolaropoulos L. 2020, PhRvD, 102, 023520
- Khadka N. & Ratra B. 2020, MNRAS, 492, 4456
- Khodyachikh M. F. 1989, SoSAO, 61, 101
- Kim J. & Naselsky P. 2010, ApJL, 714, L265
- King J. A., et al. 2012, MNRAS, 422, 3370
- Koivisto T. & Mota D. F. 2008, JCAP, 2008, 018
- Li X., Lin H.-N., Wang S. & Chang Z. 2013, EPJC, 73, 2653
- Lin H.-N., Li X. & Chang Z., 2016, MNRAS, 460, 617
- Lin H.-N., Wang S., Chang Z. & Li X. 2016, MNRAS, 456, 1881
- Lineweaver C. H., et al. 1996, ApJ, 470, 38
- Lusso E. 2020, FrASS, 7, 8
- Lusso E., et al. 2010, A&A, 512, A34
- Lusso E., et al. 2019, A&A, 628, L4
- Lusso E. & Risaliti G. 2016, ApJ, 819, 154
- Lusso E. & Risaliti G. 2017, A&A, 602, A79
- Mariano A. & Perivolaropoulos L. 2012, PhRvD, 86, 083517
- Melia F. 2019, MNRAS, 489, 517
- Migkas K., et al. 2020, A&A, 636, A15
- Päris I., et al. 2017, A&A, 597, A79
- Pelgrims V. & Hutsemékers D. 2016, A&A, 590, A53
- Perivolaropoulos L. 2014, Galaxies, 2, 22
- Planck Collaboration, et al. 2014a, A&A, 571, A23
- Planck Collaboration, et al. 2014b, A&A, 571, A26
- Qiang D.-C., Deng H.-K. & Wei H. 2019, arXiv, arXiv:1902.03580
- Qin Y. P., et al. 1997, Ap&SS, 253, 19
- Quartin M. & Notari A. 2015, JCAP, 2015, 008
- Reid B. A., et al. 2010, MNRAS, 404, 60
- Risaliti G. & Lusso E. 2015, ApJ, 815, 33
- Risaliti G. & Lusso E. 2019, NatAs, 3, 272
- Rubart M. & Schwarz D. J. A&A, 2013, 555, A117
- Salvestrini F., et al. 2019, A&A, 631, A120
- Schwarz D. J. & Weinhorst B. 2007, A&A, 474, 717
- Scolnic D. M., et al. 2018, ApJ, 859, 101
- Shen Y., et al. 2011, ApJS, 194, 45
- Singal A. K. 2011, ApJL, 742, L23
- Singal A. K. 2019, PhRvD, 100, 063501
- Sun Z. Q. & Wang F. Y. 2018, MNRAS, 478, 5153
- Sun Z. Q. & Wang F. Y. 2019, EPJC, 79, 783
- Suzuki N., et al. 2012, ApJ, 746, 85
- Tegmark M., de Oliveira-Costa A. & Hamilton A. J. 2003, PhRvD, 68, 123523
- Tiwari P. & Nusser A. 2016, JCAP, 03, 062
- Tiwari P. & Jain P. 2019 A&A, 622, A113
- Trujillo-Gomez S., Klypin A., Primack J. & Romanowsky A. J. 2011, ApJ, 742, 16
- Vagnetti F., Antonucci M. & Trevese D. 2013, A&A, 550, A71
- Velten H. & Gomes S. 2020, PhRvD, 101, 043502
- Wang F.-Y., Dai Z. G. & Liang E. W. 2015, New Astronomy Reviews, 67, 1
- Wang J. S. & Wang F. Y. 2014, MNRAS, 443, 1680
- Wang Y.-Y. & Wang F. Y. 2018, MNRAS, 474, 3516
- Watkins R., Feldman H. A. & Hudson M. J. 2009, MNRAS, 392, 743
- Webb J. K., et al. 2011, PhRvL, 107, 191101
- Wei J.-J. & Melia F. 2020, ApJ, 888, 99
- Weinberg S. Cosmology (Oxford University Press, Oxford, 2008)
- Weinberg S. Gravitation and Cosmology (Wiley, New York, 1972)
- Yang X., Wang F. Y. & Chu Z. 2014, MNRAS, 437, 1840
- Yoon, M., et al. 2014, MNRAS, 445, L60
- Yu H. & Wang F. Y. 2017, A&A, 606, A3
- Zhao W. 2014, PhRvD, 89, 023010
- Zhao W., Wu P. & Zhang Y. 2013, IJMPD, 22, 1350060
- Zhao D., Zhou Y. & Chang Z. 2019, MNRAS, 486, 5679
- Zhou Y., Zhao Z.-C. & Chang Z. 2017, ApJ, 847, 86

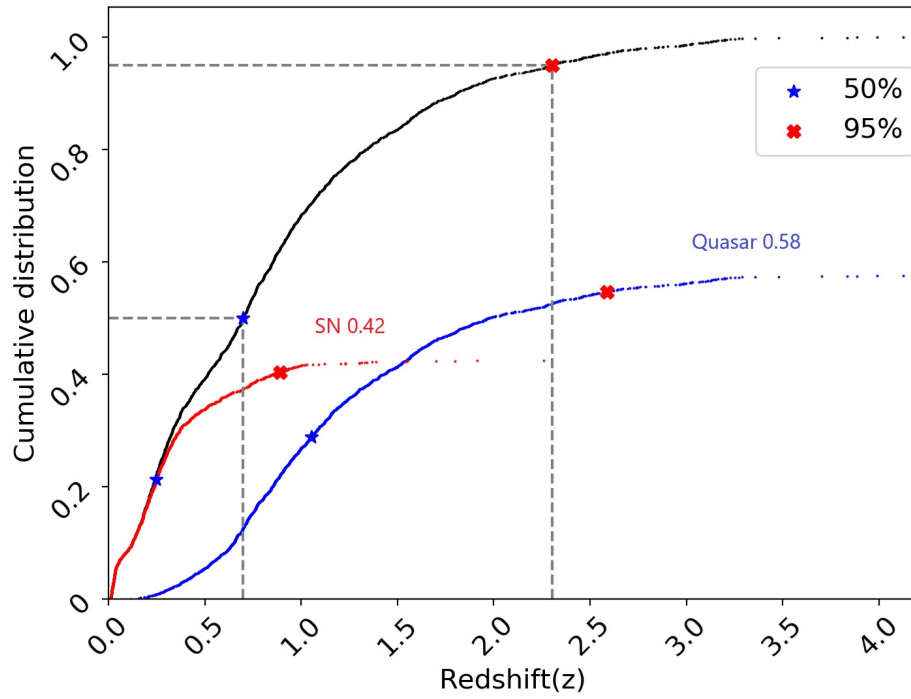
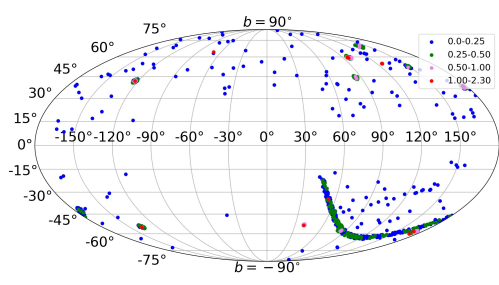
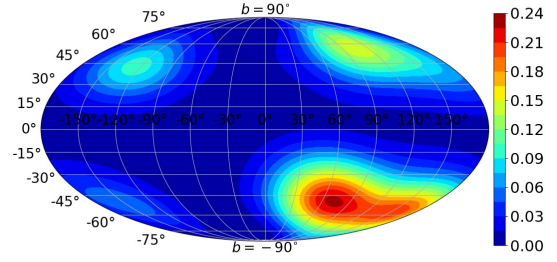


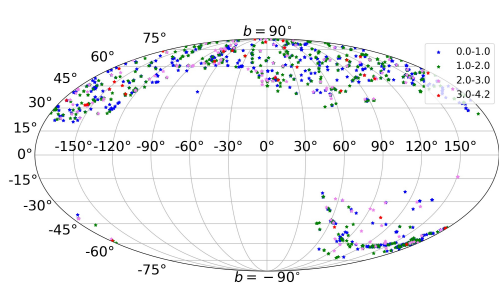
Fig. 1. Redshift cumulative distributions. Red, blue, and black lines correspond to the Pantheon, quasar, and SN-Q samples, respectively. The SNe Ia account for 42% of the SN-Q sample and the quasars for 58%.



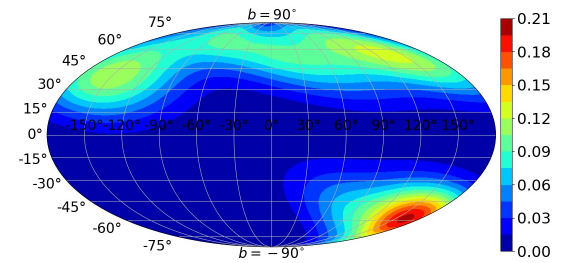
(a) Pantheon sample



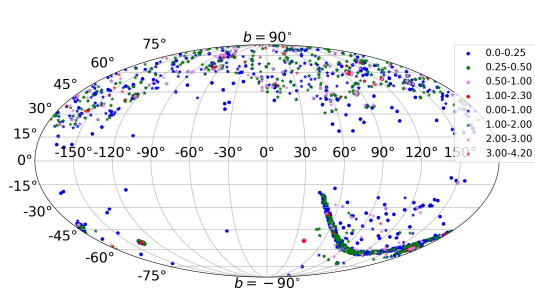
(b) Pantheon sample



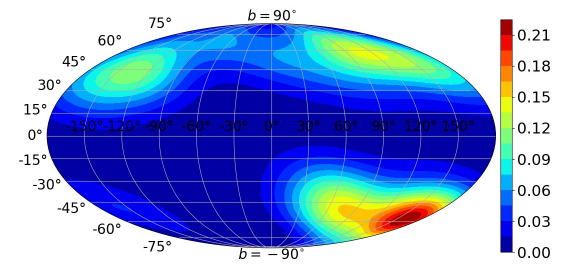
(c) The quasar sample



(d) The quasar sample



(e) SN-Q sample



(f) SN-Q sample

Fig. 2. Distributions and density contours in the galactic coordinate system. Panels (a), (c), and (e) are the coordinate distributions of the Pantheon, quasar, and SN-Q samples in the galactic coordinate system, respectively. The corresponding density contours are described in panels (b), (d), and (f).

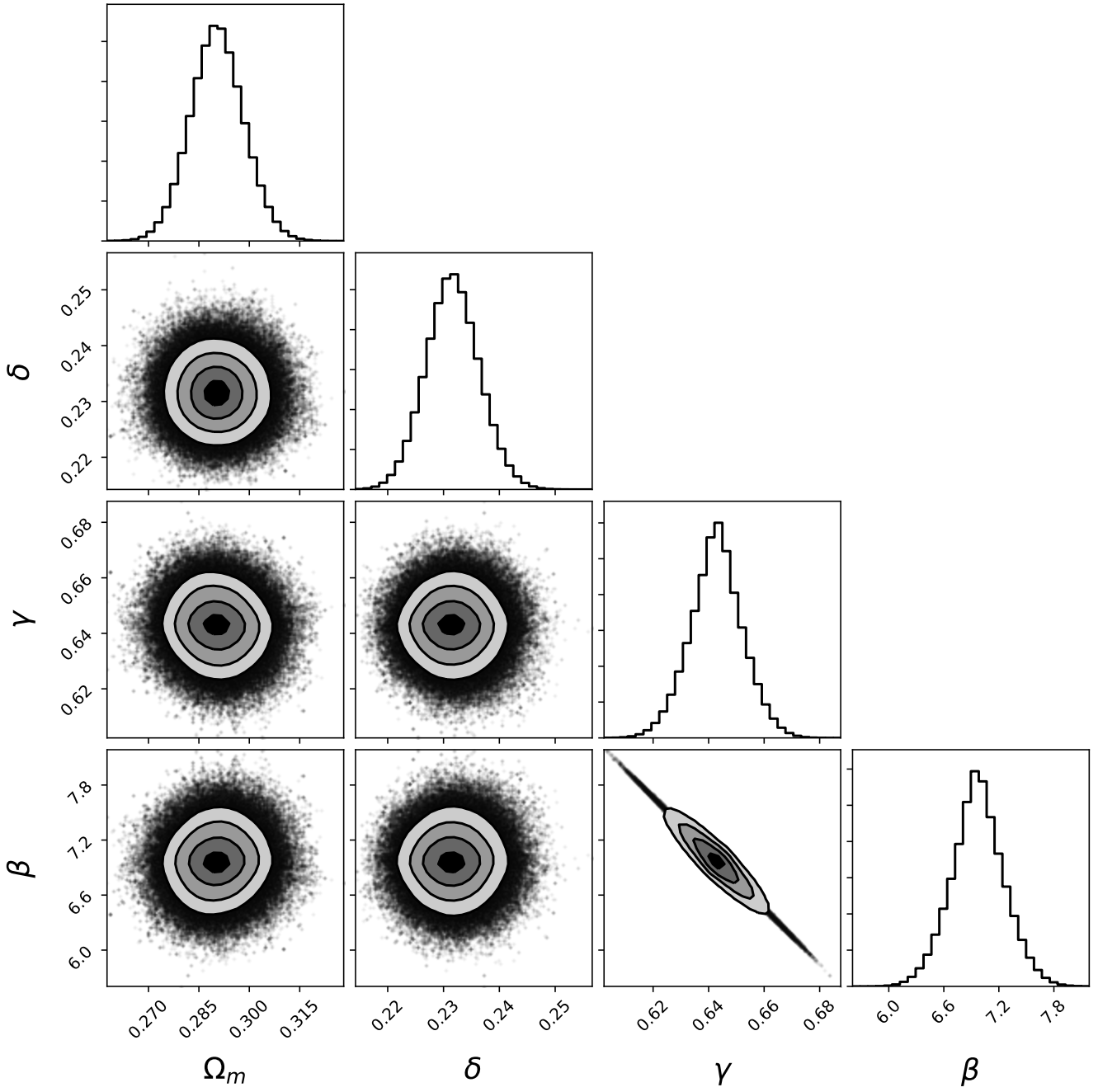


Fig. 3. Confidence contours (1σ , 2σ , and 3σ) and the marginalized likelihood distributions for the space of the parameters (Ω_m , δ , γ , β) from the SN-Q sample in the spatially flat Λ CDM model.

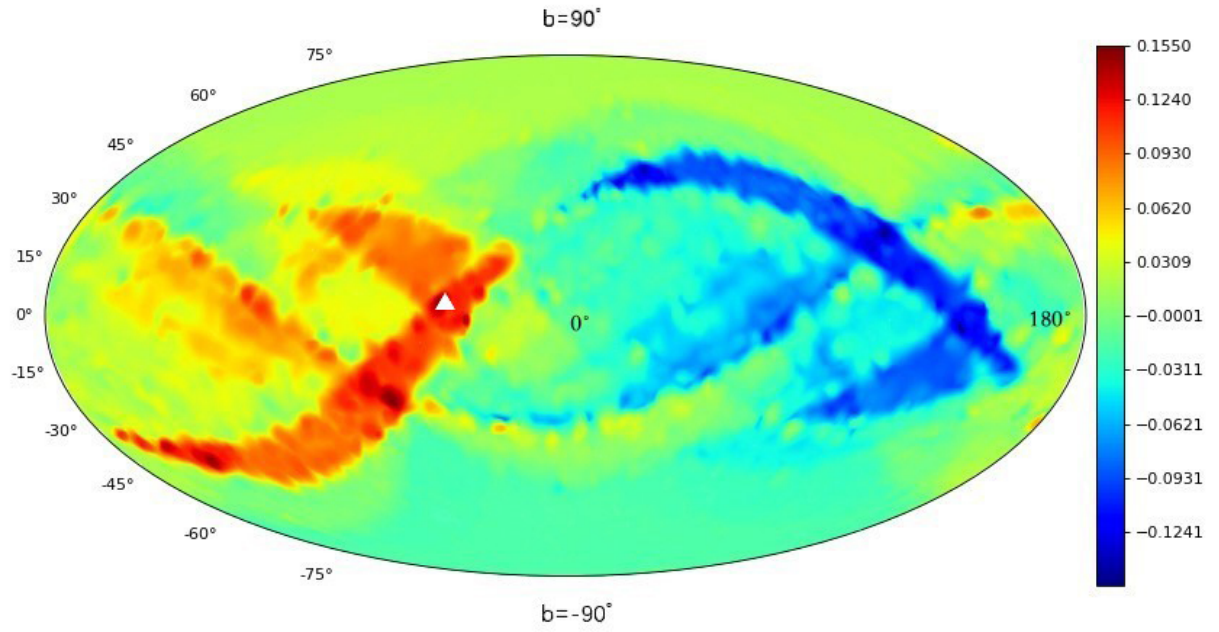


Fig. 4. Distribution of the AL in the galactic coordinate system. The triangle marks the direction of the largest of the AL in the sky.

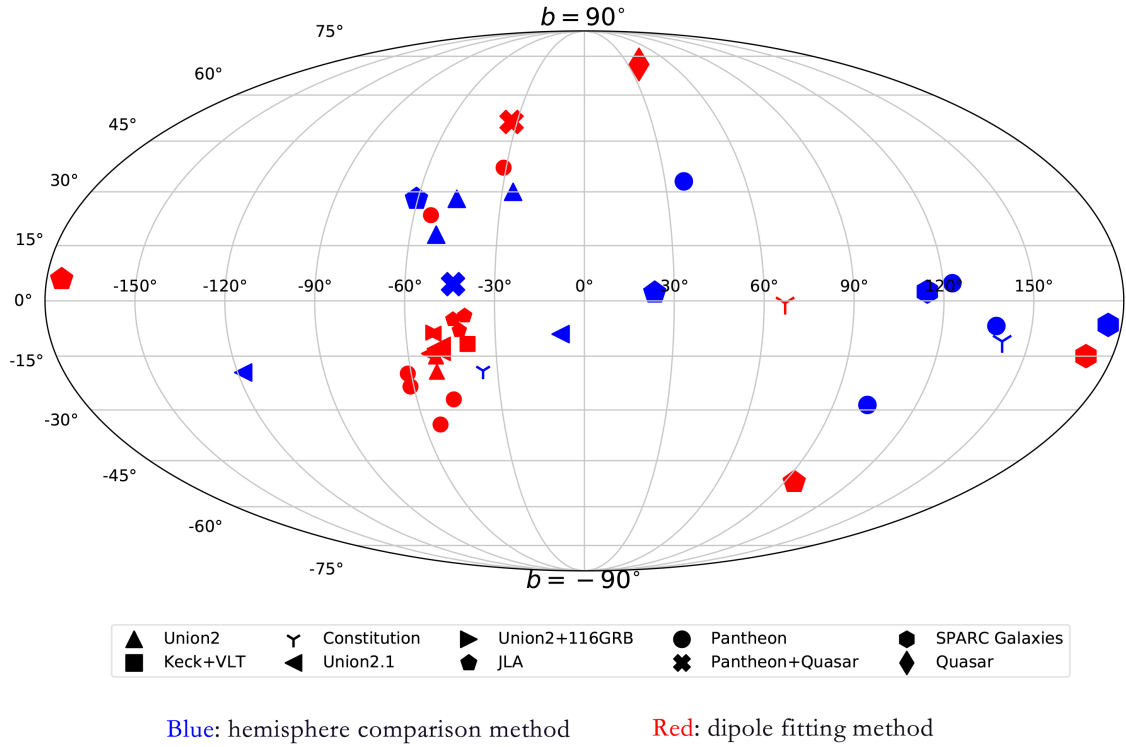


Fig. 5. Distribution of the preferred directions (l , b) in the various observational datasets. The blue color and red color correspond to the HC method and the DF method, respectively.

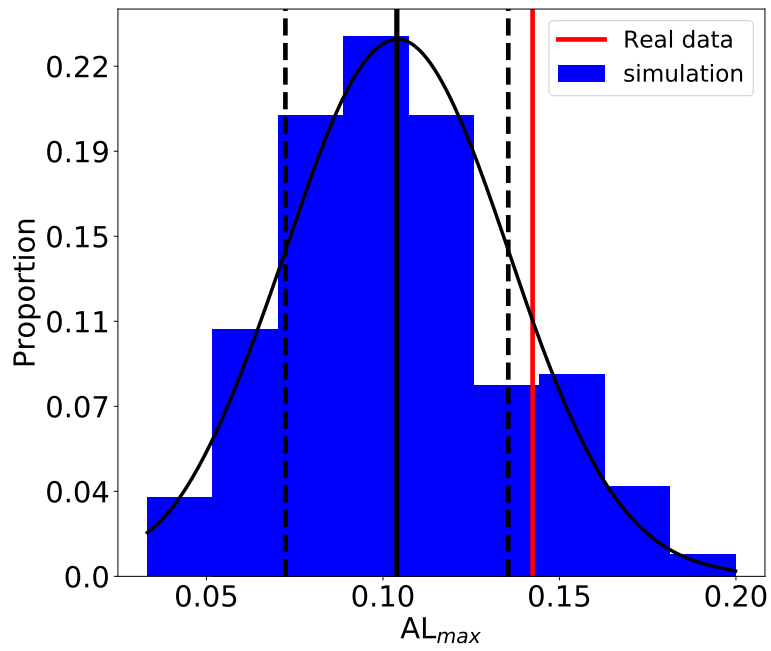


Fig. 6. Distribution of AL_{max} in 200 simulated datasets. The black curve is the best fitting result to the Gaussian function. The solid black and vertical dashed lines are commensurate with the mean and the standard deviation, respectively. The vertical red line shows the maximum AL derived from the actual SN-Q sample.

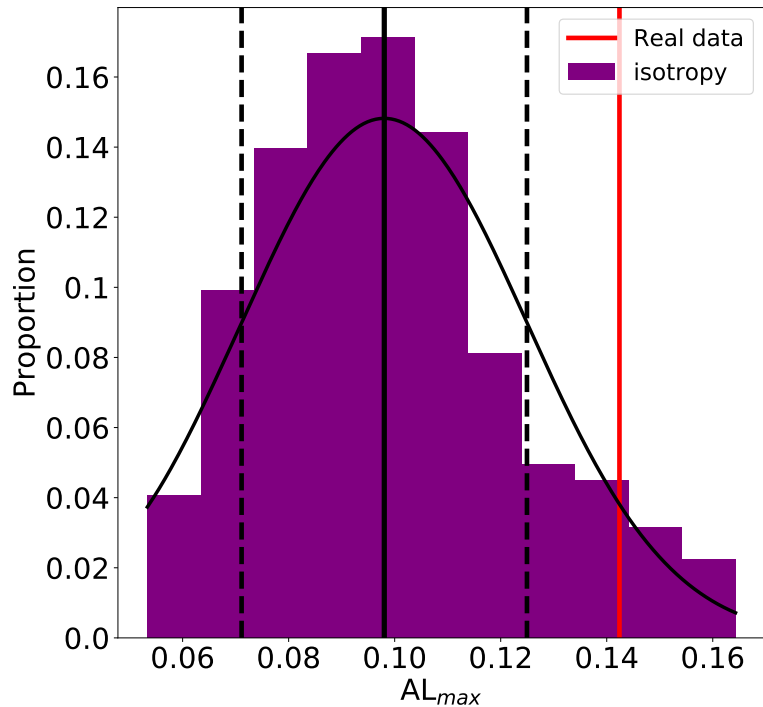


Fig. 7. Distribution of AL_{max} in 200 simulated isotropic datasets. The black curve is the best fitting result to the Gaussian function. The solid black and vertical dashed lines are commensurate with the mean and the standard deviation, respectively. The vertical red line shows the maximum AL derived from the actual SN-Q sample.

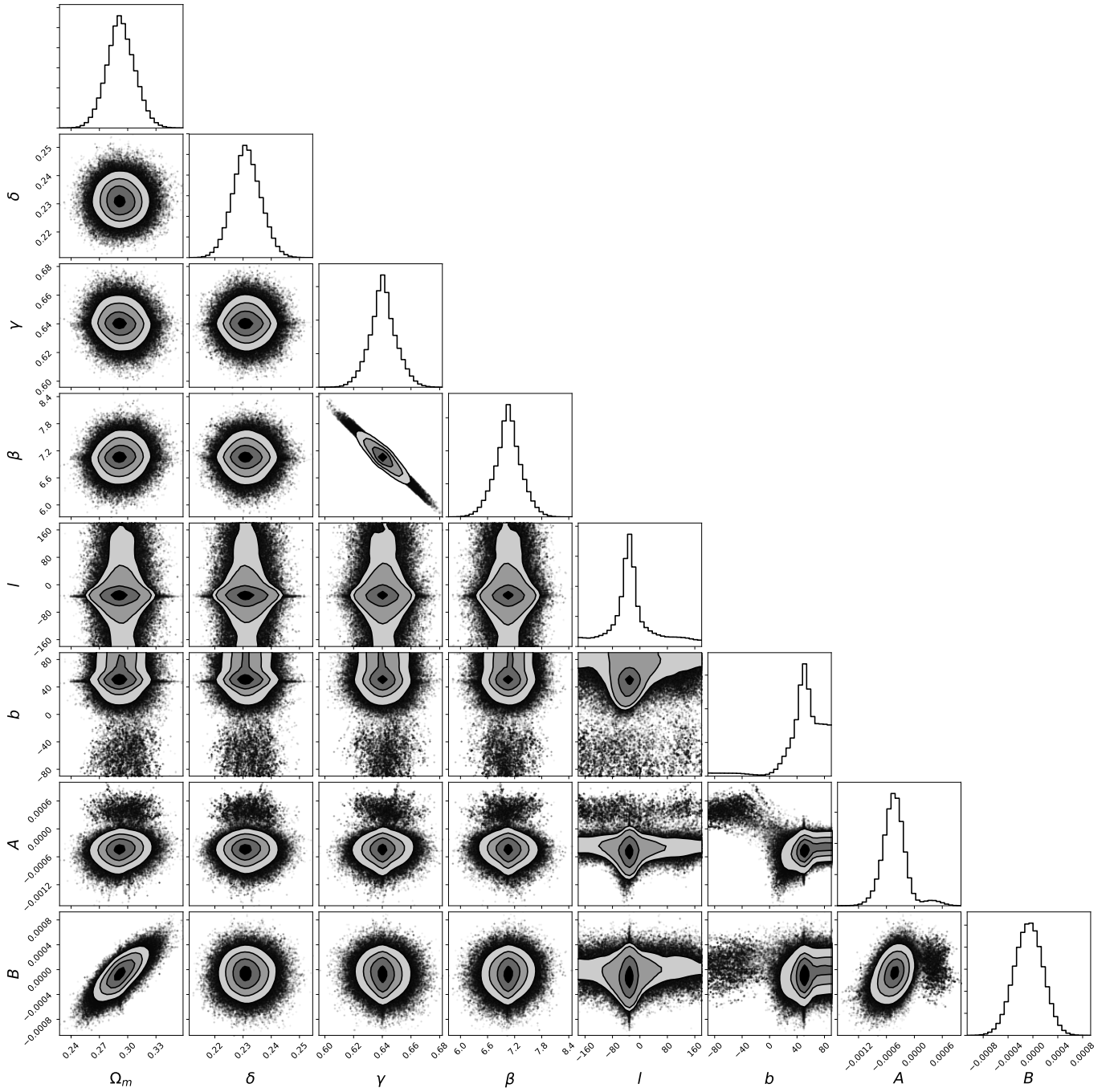


Fig. 8. Confidence contours (1σ , 2σ , and 3σ) and marginalized likelihood distributions for the parameters space (Ω_m , δ , γ , β , l , b , A , B) to the SN-Q sample in the dipole-modulated Λ CDM model.

Table 1. Preferred directions (l , b) found in different cosmological models using different methods and observational datasets.

Cosmological Obs.	Model	Method	l ($^\circ$)	b ($^\circ$)	Ref.
Union2	Λ CDM	HC	309^{+23}_{-3}	18^{+11}_{-10}	Antoniou & Perivolaropoulos (2010)
	Λ CDM	-	309°	19°	Colin, et al. (2011)
	Λ CDM	HC	314^{+20}_{-13}	28^{+11}_{-33}	Cai & Tuo (2012)
	Λ CDM	DF	$309.4^\circ \pm 18.0$	$-15.1^\circ \pm 11.5$	Mariano & Perivolaropoulos (2012)
	Λ CDM	HC	334^{+6}_{-6}	30^{+2}_{-8}	Chang & Lin (2015)
	Λ CDM	DF	$309^\circ \pm 22.4$	$-19.3^\circ \pm 12.9$	Chang & Lin (2015)
	Λ CDM	AM	126^{+17}_{-26}	13^{+19}_{-25}	Cai, et al. (2013)
67GRB	Λ CDM	AM	336^{+33}_{-223}	-5^{+34}_{-26}	Cai, et al. (2013)
	w CDM	AM	340^{+35}_{-227}	-4^{+34}_{-30}	Cai, et al. (2013)
	CPL	AM	339^{+26}_{-224}	-6^{+34}_{-25}	Cai, et al. (2013)
Union2+67GRB	Λ CDM	AM	129^{+16}_{-23}	16^{+17}_{-10}	(Cai, et al. 2013)
	w CDM	AM	129^{+17}_{-21}	15^{+18}_{-11}	Cai, et al. (2013)
	CPL	AM	131^{+14}_{-22}	16^{+15}_{-10}	Cai, et al. (2013)
Union2 + SN _{FACTORY}	Λ CDM	DF (z,0.015-0.035)	$298^\circ \pm 25$	$15^\circ \pm 20$	Feindt, et al. (2013)
	Λ CDM	DF (z,0.035-0.045)	$302^\circ \pm 48$	$-12^\circ \pm 26$	Feindt, et al. (2013)
	Λ CDM	DF (z,0.045-0.060)	$359^\circ \pm 32$	$14^\circ \pm 27$	Feindt, et al. (2013)
	Λ CDM	DF (z,0.060-0.100)	$285^\circ \pm 234$	$-23^\circ \pm 112$	Feindt, et al. (2013)
Union2.1	Λ CDM	HC	-	-	Yang, Wang & Chu (2014)
	Λ CDM	DF	$307.1^\circ \pm 16.2$	$-14.3^\circ \pm 10.1$	Yang, Wang & Chu (2014)
	Λ CDM	HC	241.9°	-19.5°	(Lin, Li & Chang 2016)
	Λ CDM	DF	$310.6^\circ \pm 18.2$	$-13.0^\circ \pm 11.1$	Lin, Li & Chang (2016)
	Λ CDM	Hubble map	326.25°	12.02°	Bengaly, Bernui & Alcaniz (2015)
	Λ CDM	q map	354.38°	27.28°	Bengaly, Bernui & Alcaniz (2015)
	Λ CDM	HC	352°	-9°	Sun & Wang (2019)
	Λ CDM	DF	$309.3^{+15.5}_{-15.7}$	$-8.9^{+11.2}_{-9.8}$	Sun & Wang (2019)
Union2.1+116GRB	Λ CDM	DF	$309.2^\circ \pm 15.8$	$-8.6^\circ \pm 10.5$	Wang & Wang (2014)
Keck+VLT	Λ CDM	DF	$320.5^\circ \pm 11.8$	$-11.7^\circ \pm 7.5$	Mariano & Perivolaropoulos (2012)
Constitution	Λ CDM	HC	-35°	-19°	Kalus, et al. (2013)
	Λ CDM	HC	141°	-11°	Sun & Wang (2019)
	Λ CDM	DF	$67.0^{+66.5}_{-66.2}$	$-0.6^{+25.2}_{-26.3}$	Sun & Wang (2019)
JLA	Λ CDM	Hubble map	58.00°	-60.43°	Bengaly, Bernui & Alcaniz (2015)
	Λ CDM	q map	225.00°	51.26°	Bengaly, Bernui & Alcaniz (2015)
	Λ CDM	HC(max)	23.49°	2.25°	Deng & Wei (2018)
	Λ CDM	HC(submax)	299.47°	28.39°	Deng & Wei (2018)
	Λ CDM	DF	185^{+175}_{-185}	$5.9^{+84.1}_{-95.9}$	Deng & Wei (2018)
	Λ CDM	DF	316^{+107}_{-100}	-5^{+41}_{-60}	Lin et al. (2016)
	w CDM	DF	320^{+107}_{-104}	-4^{+45}_{-61}	Lin et al. (2016)

	CPL Λ CDM	DF DF	318^{+177}_{-183} 94.4°	-8^{+36}_{-54} -51.7°	Lin et al. (2016) Sun & Wang (2019)
Pantheon	Λ CDM	HC	$37^\circ \pm 40$	$33^\circ \pm 16$	Sun & Wang (2018)
	Λ CDM	DF	329^{+101}_{-28}	37^{+52}_{-21}	Sun & Wang (2018)
	Λ CDM	HC(max)	$138.08^{+3.16}_{-16.90}$	$-6.8^{+13.55}_{-2.31}$	Deng & Wei (2018)
	Λ CDM	HC(submax)	$102.36^{+47.95}_{-34.22}$	$-28.58^{+50.60}_{-1.78}$	Deng & Wei (2018)
	Λ CDM	DF	-	-	Deng & Wei (2018)
	Λ CDM	HC	$123.05^{+11.25}_{-4.22}$	$4.78^{+1.80}_{-8.36}$	Zhao, Zhou & Chang (2019)
	Λ CDM	DF	$306.00^{+82.95}_{-125.01}$	$-34.20^{+16.82}_{-54.93}$	Zhao, Zhou & Chang (2019)
	Λ CDM	HC	$286.93^\circ \pm 18.52^\circ$	$27.02^\circ \pm 6.5^\circ$	Kazantzidis & Perivolaropoulos (2020)
	Λ CDM	DF	$210.25^\circ \pm 136.56^\circ$	$72.85^\circ \pm 60.63^\circ$	Kazantzidis & Perivolaropoulos (2020)
	Λ CDM	DF	$306.00^{+91.94}_{-125.98}$	$-23.41^{+22.97}_{-54.71}$	Chang & Zhou (2019)
w CDM	DF	$298.81^{+84.18}_{-118.71}$	$-19.80^{+14.07}_{-63.25}$	Chang & Zhou (2019)	
CPL	DF	$313.20^{+75.30}_{-133.15}$	$-27.00^{+18.72}_{-57.24}$	Chang & Zhou (2019)	
Finslerian	DF	$298.80^{+75.31}_{-118.69}$	$-23.41^{+19.26}_{-57.41}$	Chang & Zhou (2019)	
CMB Dipole	-	-	$263.99^\circ \pm 0.14$	$48.26^\circ \pm 0.03$	Lineweaver, et al. (1996)
Velocity Flows	-	-	282°	6°	Watkins, Feldman & Hudson (2009), Watkins, Feldman & Hudson (2009), Feldman, Watkins & Hudson (2010)
Quasar Alignment	-	-	267°	69°	Hutsemékers & Lamy (2001), Hutsemékers, et al. (2005), Hutsemékers, et al. (2011)
CMB Octopole	-	-	308°	63°	Bielewicz, Górski & Banday (2004)
CMB Quadrupole	-	-	240°	63°	Bielewicz, Górski & Banday (2004), Frommert & Enßlin (2010)
$\Delta\alpha/\alpha$	-	-	330°	-13°	Webb, et al. (2011) , King, et al. (2012)
SPARC Galaxies	-	HC(max)	175.5°	-6.5°	Zhou, Zhao & Chang (2017)
	-	HC(submax)	114.5°	2.5°	Zhou, Zhao & Chang (2017)
	-	DF	171°	-15°	Chang, et al. (2018)
Galaxy Cluster	Λ CDM	-	303°	-27°	Migkas, et al. (2020)
Infrared galaxies	-	-	310°	-15°	Yoon, et al. (2014)
	-	HC	323°	-5°	Bengaly, et al. (2017)
Pantheon+1421Quasar	Λ CDM	HC	$316.08^{+27.41}_{-129.48}$	$4.53^{+26.29}_{-64.06}$	this paper
	Λ CDM	DF	$327.55^\circ \pm 32.45$	$51.01^\circ \pm 26.50$	this paper

Table 2. Redshift tomography results using dipole fitting method for the SN-Q sample.

	$N_{\text{SN+Quasar}}$	Ω_m	δ	γ	β	l ($^\circ$)	b ($^\circ$)	A	B
$z < 0.25$	21 + 530	$0.285^{+0.049}_{-0.073}$	$0.295^{+0.05}_{-0.06}$	$0.628^{+0.098}_{-0.105}$	$7.747^{+3.52}_{-4.03}$	$279.88^{+12.15}_{-26.71}$	$23.76^{+25.29}_{-16.94}$	$-8.43^{+3.32}_{-6.59}e-4$	$-2.84^{+3.19}_{-5.11}e-4$
$z < 0.50$	136 + 832	$0.273^{+0.024}_{-0.035}$	$0.261^{+0.017}_{-0.022}$	$0.576^{+0.044}_{-0.065}$	$9.007^{+1.36}_{-1.83}$	$306.98^{+20.96}_{-20.16}$	$30.95^{+34.52}_{-16.01}$	$-3.98^{+3.01}_{-5.14}e-4$	$-2.20^{+2.52}_{-4.30}e-4$
$z < 0.75$	379 + 949	$0.285^{+0.018}_{-0.027}$	$0.237^{+0.008}_{-0.012}$	$0.615^{+0.027}_{-0.037}$	$7.829^{+0.079}_{-1.12}$	$319.09^{+30.80}_{-38.48}$	$40.33^{+29.86}_{-18.70}$	$-4.58^{+2.10}_{-3.90}e-4$	$-1.40^{+2.17}_{-3.73}e-4$
$z < 1.00$	664 + 1025	$0.285^{+0.014}_{-0.020}$	$0.238^{+0.006}_{-0.009}$	$0.633^{+0.019}_{-0.026}$	$7.302^{+0.56}_{-0.81}$	$321.78^{+26.27}_{-37.19}$	$52.78^{+23.41}_{-13.84}$	$-4.65^{+1.75}_{-3.14}e-4$	$-1.32^{+2.02}_{-3.26}e-4$
$z < 1.50$	1020 + 1042	$0.289^{+0.013}_{-0.019}$	$0.235^{+0.005}_{-0.008}$	$0.633^{+0.013}_{-0.019}$	$7.294^{+0.42}_{-0.56}$	$324.72^{+27.61}_{-23.42}$	$45.83^{+24.09}_{-14.43}$	$-4.67^{+1.64}_{-3.19}e-4$	$-9.40^{+19.5}_{-32.1}e-5$
$z < 2.50$	1334 + 1048	$0.293^{+0.013}_{-0.019}$	$0.233^{+0.0046}_{-0.0068}$	$0.630^{+0.0010}_{-0.014}$	$7.367^{+0.309}_{-0.425}$	$322.44^{+34.89}_{-31.42}$	$47.40^{+24.75}_{-13.72}$	$-4.47^{+1.64}_{-3.06}e-4$	$-5.30^{+19.1}_{-32.0}e-5$
$z < 3.50$	1416 + 1048	$0.294^{+0.0051}_{-0.019}$	$0.232^{+0.0019}_{-0.0066}$	$0.641^{+0.0034}_{-0.0124}$	$7.059^{+0.104}_{-0.375}$	$325.38^{+32.01}_{-35.23}$	$50.93^{+24.69}_{-10.63}$	$-4.12^{+0.66}_{-2.97}e-4$	$-3.10^{+0.76}_{-3.15}e-5$
$z < 4.20$	1421 + 1048	$0.292^{+0.015}_{-0.017}$	$0.231^{+0.005}_{-0.006}$	$0.640^{+0.009}_{-0.011}$	$7.041^{+0.28}_{-0.34}$	$327.21^{+28.24}_{-27.50}$	$48.67^{+8.99}_{-8.44}$	$-4.36^{+1.98}_{-2.74}e-4$	$-6.60^{+21.5}_{-28.6}e-5$